

## Using of ASTER, ETM+ and Gamma Spectrometry Airborne Data to Find the Relationship Between the Distribution of Alkali Metasomatism and REE Mineralization in the Bafq Area, Central Iran

K. Khoshnoodi<sup>\*1,2</sup>, M. Yazdi<sup>1</sup>, M. Gannadi-Maragheh<sup>2</sup>, and M. Behzadi<sup>1</sup>

<sup>1</sup> Department of Geology, Faculty of Earth Science, University of Shahid Beheshti, Tehran, Islamic Republic of Iran

<sup>2</sup> Nuclear Science and Technology Research Institute, Atomic Energy Organization of Iran, Tehran, Islamic Republic of Iran

Received: 17 January 2015 / Revised: 27 July 2015 / Accepted: 7 November 2015

### Abstract

The study area is located in the central Iranian tectono-magmatic zone, which is known for its world-class IOA-type Iron ore deposits. The Advanced Space borne Thermal Emission and Reflection Radiometer (ASTER) and Landsat Enhanced Thematic Mapper Plus (ETM+) image-processing techniques, were used in satellite imagery through conventional and also modern processing methods including band ratios, color composite ratio images and spectral angle mapper to study the spectral discrimination of metasomatically altered rocks based on their mineral assemblages and to investigate critically the link between the distribution of Na-metasomatism and occurrence of REE mineralization through plotting the image processing results on preexisting airborne radiometric data. The achieved information points the matter that the distribution of the metasomatized rocks, in common, and Na-metasomatized rocks, in particular, are coincide with the areas with high radioactivity revealed during an airborne radiometry program. A stage of field study associated with ground spectrometry survey carried out to control some localities and showed such correlation mainly around and within some magnetite ore deposits through which two phases of albitization were revealed, namely, a widespread albitization phase within which the spectrometric survey showed normal amounts of radioactive elements and another phase that affected smaller areas and showed REE anomaly and the Na-metasomatites of which are, experimentally, more reddish in colure (meaty color in hand specimens). The Iron deposits are, chronologically, hosted in upper Proterozoic-lower Cambrian volcano-magmatic units associated with a widespread phase of Na-metasomatism, economically, resulted in enrichment of the host rocks in REE bearing mineral phases.

**Keywords:** ASTER and ETM+ data; Na-metasomatism; REE mineralization; central Iran.

\* Corresponding author: Tel: +982182062522; Fax: +982182062521; Email: khoshnoodi78@gmail.com

## Introduction

The central lithotectonic domain of the Posht-e-Badam Block, within the Central Iranian microcontinent, contains the oldest (Late Neoproterozoic) basement of Iran. The Bafq mining district is located in the southern section of this lithotectonic domain (Fig. 1a) and hosts abundant mineral deposits, particularly those of the iron oxide-apatite (IOA), Fe-Mn exhalative, and Zn-Pb sedimentary-exhalative (SEDEX) types, being one of the main metallogenic provinces in Iran. The Bafq mining district also known as the Zarigan-Chahmir basin and its ore deposits have been the subject of many geological studies (Daliran, [11]; Daliran et al., [12, 13]; Förster and Jafarzadeh, [17]; Mohammad torab et al. [31], Nadimi, [32]; Rajabi, [34, 35]; Rajabi et al., [36, 37]; Ramezani and Tucker, [38]; Stosch et al., [45]; Yaghubpour and Mehrabi, [50]). Some of iron oxide-apatite (IOA) ore deposits of Bafq contain REE-U-Th(REE-U/Th) mineralization. The Bafq iron ore deposits show a spectrum of mineralization styles like massive ore bodies, metasomatic replacements, veins and stockworks, of which their distribution varies considerably within the individual deposits [31]. Of important matter in the Bafq mining district is the occurrence of REE-Th (in Choghart mine) and, REE-U-Th (anomaly 5 in the Saghand ore field) mineralization in peripheral alteration zones around the Iron ore deposits also the correlation between the areas containing such metals and the distribution of the rocks affected by alkali metasomatism. Narigan ore deposit is an exception in which U-Mo mineralization has, genetically, a granite related origin [24]. U-Mo mineralization in the Narigan ore deposit is not related to hydrothermal processes. Metasomatic processes are proposed to play geochemical roles in concentration of REE-U-Th bearing minerals in some part of the world. Na-metasomatism, among several types of metasomatic processes, results more effectively in concentration of such elements. This aspect of metasomatism is characterized by Na-bearing minerals, which are clearly in replacement relationships with primary magmatic minerals [33]. The metasomatic and hydrothermal processes that take place with aqueous solutions are the only endogenic processes in which the concentration of radioactive elements, and primarily uranium, reach industrial concentration [47]. The rocks affected by this type of metasomatism were first described as Na-granites by Tanatar [46] or as syenites by Feldman [15]. There has been an ongoing interest in the association of REE, Th and U mineralization and this type of metasomatism due, with no doubt, to the importance of

the albitization in mineralization of radioactive elements. According to Kinnaird [27] Na-enrichment is accompanied by concentrations of Fe, U, Th, Zr, Nb, Sn, Zn and HREE. Also, Na-metasomatized rocks tend to be enriched with respect to K-metasomatized rocks in Rb, Th, Nb, La, Ce, Hf, Zr, and Y. Some localities of the world have been studied in which the mineralization of the radioactive elements is controlled by the occurrence and development of the albitites like central Ukraine [9] and the Uranium city region in Canada [10]. High-temperature hydrothermal Th deposits are characterized by metasomatic replacements, accompanied by amphibolytization, aegirinitization, biotitization, greisenization and filled open cavities, [47]. Alkali-metasomatism in the Bafq mining district occurred in several localities mainly in peripheral alteration zones of iron ore deposits. Obtained apatite ages confirm that IOA and the apatite-rich rocks (apatites) of the Bafq district formed coevally with the Early Cambrian magmatic (-metasomatic) events [44]. With this background, the Aster images were used, critically, to evaluate the possible relationships between the distribution of the alkali-metasomatized rocks and occurrences of REE and Th mineralization through SAM method. Since REE mineralization, in the Bafq area, is generally and paragenetically associated with Th/U mineralization, the gamma spectrometric airborne data was used as an indirect method in detection of the areas hosting the REE bearing minerals.

This study aims at integrating remote sensing, airborne radiometric data and field studies to prospect for REE-Th mineralization at this district. Band rationing on the ETM+ images, in general, and spectral angle mapper (SAM) method, in particular, on the ASTER images carried out, to reveal and investigate the correlation between the distribution of the rocks affected by all types of alteration and to pointing the exact location of the areas affected by albitization and correlation with REE and Th mineralization, respectively. The procedure of the study involved field observations, global positioning system (GPS) readings, processing the images using the ENVI imagine 4.8 software, ground spectrometry, collection of samples for laboratory chemical analysis and taking field photographs and combination of the information layers in geographic information system using Arc GIS 9.3 software environment.

## Materials and Methods

### *Geological setting and mineralization*

The crustal domain referred to as the Central Iranian microcontinent is a composite of three major structural

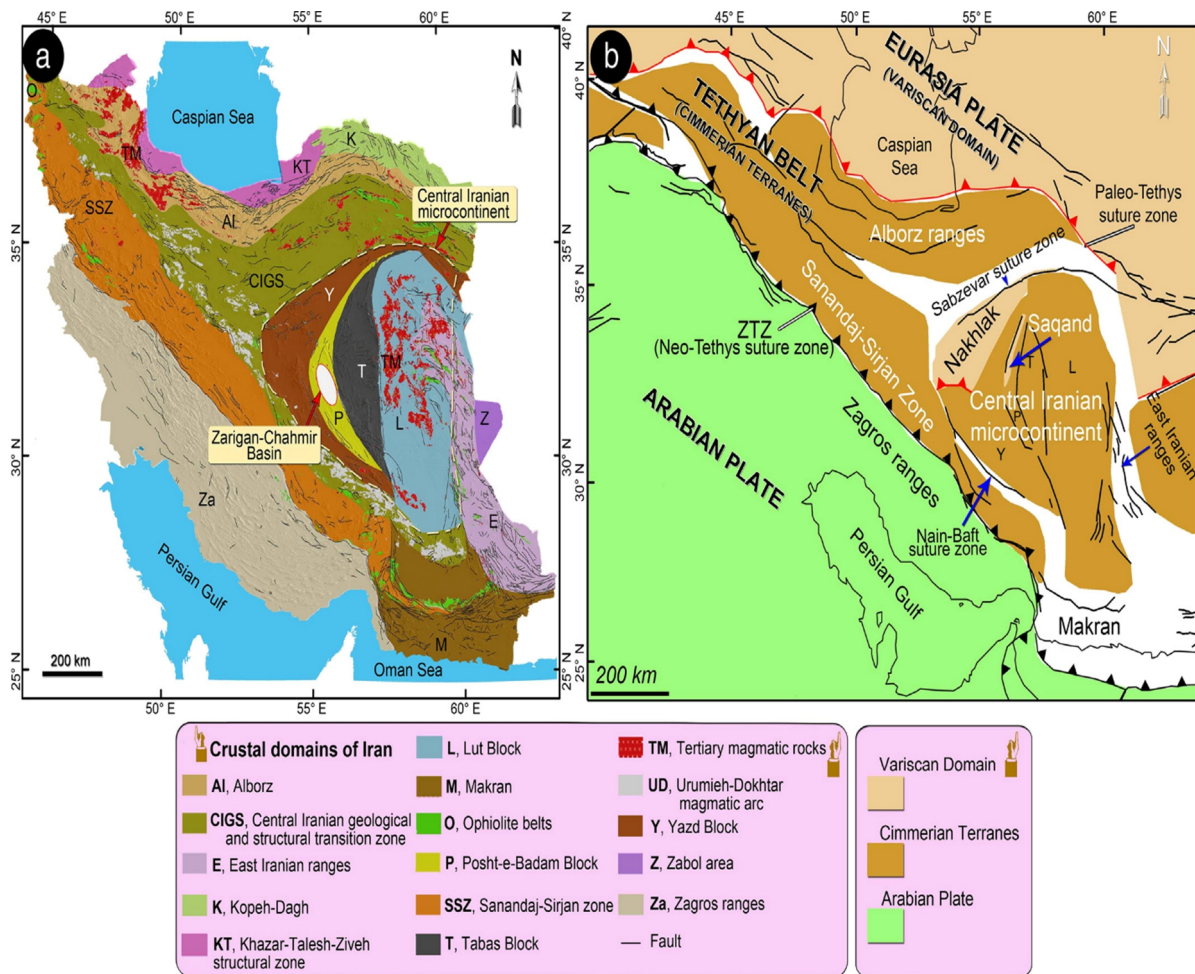


**Figure 1.** (a) Simplified structural map of Iran (Aghanabati, [1]) and location of the Zarigan–Chahmir basin/Bafq district in the Posht-e-Badam Block. (b) Eastern part of the Terranes map of the western Tethysides (Rajabi et al., [35,36]; modified by Stampfli, [43]; according to Bagheri and Stampfli, [5]). Note the location of the Iran Plate (Iranian Cimmerian terranes) between the Variscan domain in the north and the Arabian Plate in the southwest. ZTZ: Zagros Thrust Zone.

zones, from E to W [3]: the Lut, Tabas, and Yazd blocks (Fig. 1a and b). The boundaries are defined by regional-scale faults (Fig. 1). In addition, there is the Posht-e-Badam Block [3], a fault-bound, variably deformed and metamorphosed complex of supracrustal rocks that separates the Tabas and Yazd blocks (Fig. 1). The Posht-e-Badam Block is located within an area defined between three major fault systems [3]: the Chapedony, Kalmard and Kuhbanan faults. A Precambrian crystalline basement and Early Cambrian to Tertiary sedimentary cover are exposed in the block [17]. The Precambrian basement consists of medium- to high-grade metamorphic rocks, Late Neoproterozoic in age, grouped in the Boneh-Shurow and Posht-e-Badam complexes (Fig. 2, [38, 48]). The bulk of the Posht-e-Badam complex consists of a variable association of greenstones, schists, meta-greywackes, marbles,

gneisses, amphibolites, pyroxenites, serpentinites, metabasalts and conglomerates [20]. This complex is exposed west of the Posht-e-Badam Fault (Fig. 2) and is severely disrupted by Triassic granitic plutons [38]. The Boneh-Shurow complex, which is the most widely exposed metamorphic unit, crops out east of the Posht-e-Badam Fault (Fig. 2, [20]). This complex is approximately 2000 m thick and exhibits a variety of metamorphic rocks, including quartz–feldspathic gneisses, green mica–schists and amphibolites [2]. Zircon U/Pb dating of this complex indicates an age of 602–617 Ma [38]. The Boneh-Shurow complex is covered by a 2000-m-thick sequence of greywackes, quartzites and quartzitic schists, marbles, amphibolites, gneiss, slaty-shales, basaltic lavas, sandstones and arkosic arenites, argillites, tuffaceous rocks and limestones belonging to the Tashk Formation, of Late

Neoproterozoic to Early Cambrian age [38] that partly metamorphosed to the green schist facies. During the Early Cambrian, granitic plutons intruded the Precambrian sequence of the Tashk Formation, and felsic to intermediate volcanic and volcano-sedimentary rocks of the ECVSS (Early Cambrian volcano-sedimentary sequence) were deposited. The 2000–2500 m thick ECVSS unconformably overlies the clastic sedimentary and tuffaceous rocks of the Tashk Formation. This contact is well exposed to the W and SW of the Narigan area. The ECVSS has also been termed the CVSU (Cambrian Volcano-Sedimentary Unit), Rizu-Desu series and Esfordi Formation, in different parts of the area between the Posht-e-Badam and Kerman areas [19, 22, 38, 41]. The ECVSS consists of an unmetamorphosed sequence of interlayered micro-conglomerates, sandstones, mafic to felsic volcanic rocks, pyritic black siltstones and shales, volcanoclastic beds and tuffaceous shales, dolomites and dolomitic limestones [19, 35, 38]. This sequence is the host of the most important IOA [11], Fe–Mn and SEDEX Zn–Pb deposits of Iran (Fig. 2, [35, 36]). Iron oxide–apatite (IOA) deposits, often referred to as Kiruna-type iron ore deposits, are known to have formed Since the Proterozoic to the Tertiary. They are

commonly associated with calc–alkaline volcanic rocks and regional- to deposit-scale metasomatic alteration [44]. Table 1 lists the characteristics of four, economically, important IOA ore deposits in the Bafq area.

**Remote sensing data**

Remote-sensing techniques have been applied for many years, and new methodological perspectives are still being developed using this high technology [50]. Different image processing techniques such as color composites, band rationing, principal component image analysis (PCA), intensity–hue–saturation (IHS) transformation, filtering, supervised classification, and unsupervised classification are normally used for delineating are as favorable for further exploration [26]. In this study, three different processing techniques were used for detection of Na-metasomatized areas including: color composites, band rationing and spectral angle mapper. The associated zones of Na-metasomatism, in the study area, are spatially large enough to be detected and mapped using multispectral remote sensing data.

ETM+ and Aster data were processed using the ENVI imagine 4.8 software. ASTER covers a wide

**Table 1.** the characteristics of important ore deposits in the Bafq mining district [6, 45].

Deposit	Type of ore	Type of the host rock	Type of metasomatism
Esfordi	Apatite rich-iron ore	Rhyolite	Alkali metasomatism (actinolitization)
Chador Malu	Iron-apatite ore	Rhyolite (mostly altered)	Alkali metasomatism (albitization)
Choghart	Mostly rich iron ore	Rhyolite (mostly altered)	Alkali metasomatism (actinolitization and albitization)
Se-Chahun	Mostly poor iron ore	Rhyolitic tuff	Alkali metasomatism (actinolitization and albitization)

**Table 2.** Summary of performance characteristics for ASTER and ETM+ sensors (sumerized from Honarmand [21]).

Multispectral sensor	Subsystem	Band no	Spectral range(μm)	Spatial (m)
Aster	VNIR	1 (nadir)	0.52–0.60	15
		2 (nadir)	0.63–0.69	
		3 (nadir)	0.78–0.86	
	SWIR	3 (backward)	0.78–0.86	30
		4	1.600–1.700	
		5	2.145–2.185	
		6	2.185–2.225	
		7	2.235–2.285	
		8	2.295–2.365	
ETM+		9	2.360–2.430	30
		1	0.450–0.515	
		2	0.525–0.605	
		3	0.630–0.690	
		4	0.750–0.900	
		5	1.55–1.75	
		6	10.40–12.50	60
		7	2.08–2.35	
		8 (pan)	0.52–0.90	

spectral region with 14 bands from the visible to the thermal infrared with high spatial, spectral and radiometric resolution. The spatial resolution varies

with wavelength: 15 m in the visible and near-infrared (VNIR), 30 m in the short wave infrared (SWIR), and 90 m in the thermal infrared (TIR). The ETM+ image

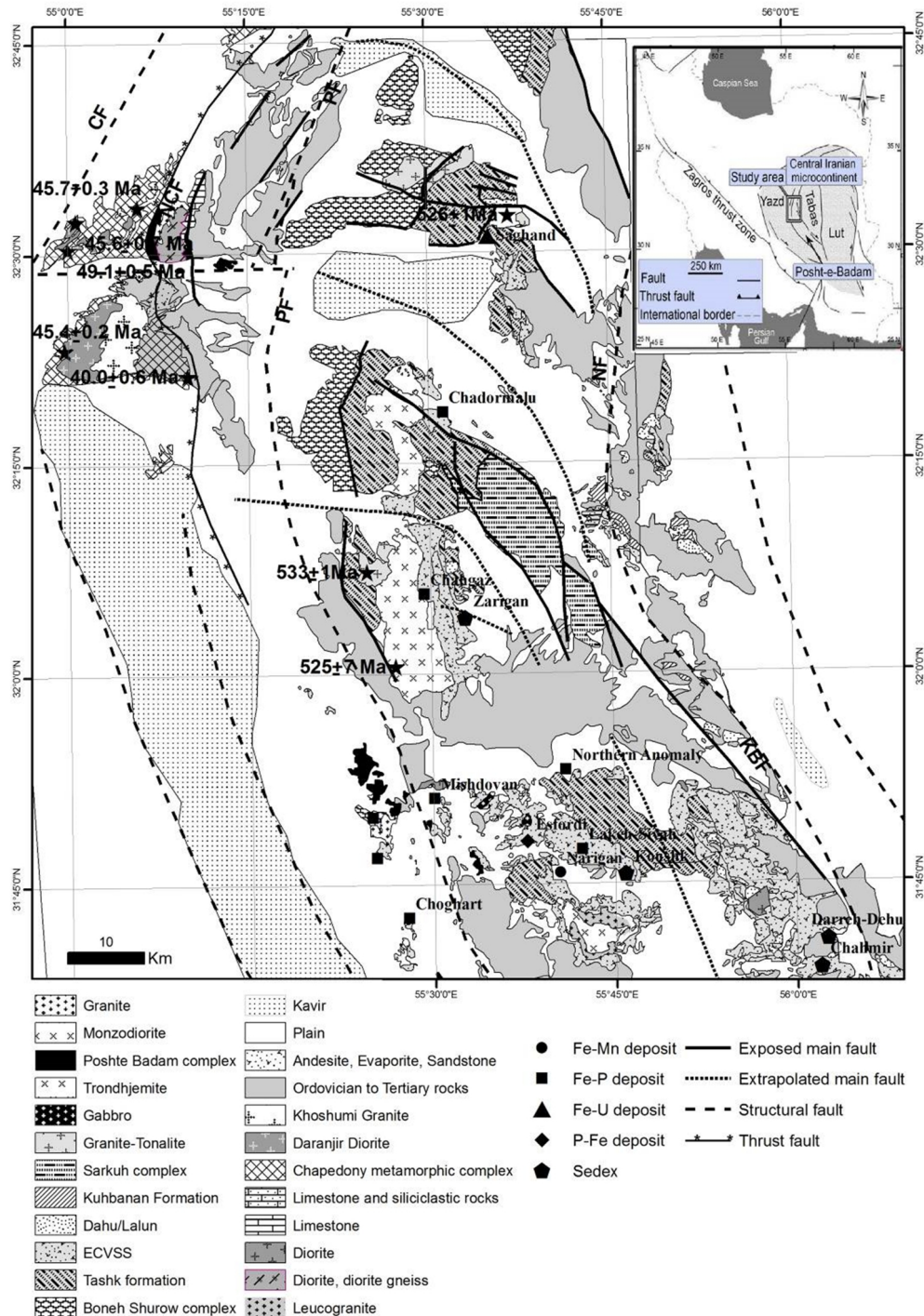


**Figure 2.** Simplified geological map of the Bafq district in the Posht-e-Badam Block, (modified after Haghypour, [19], Kargaranbafghi et al., [25] Ramezani and Tucker, [38] and Rajabi et al., [37]). Geochronological data from Ramezani and Tucker [38] and Kargaranbafghi et al., [25]

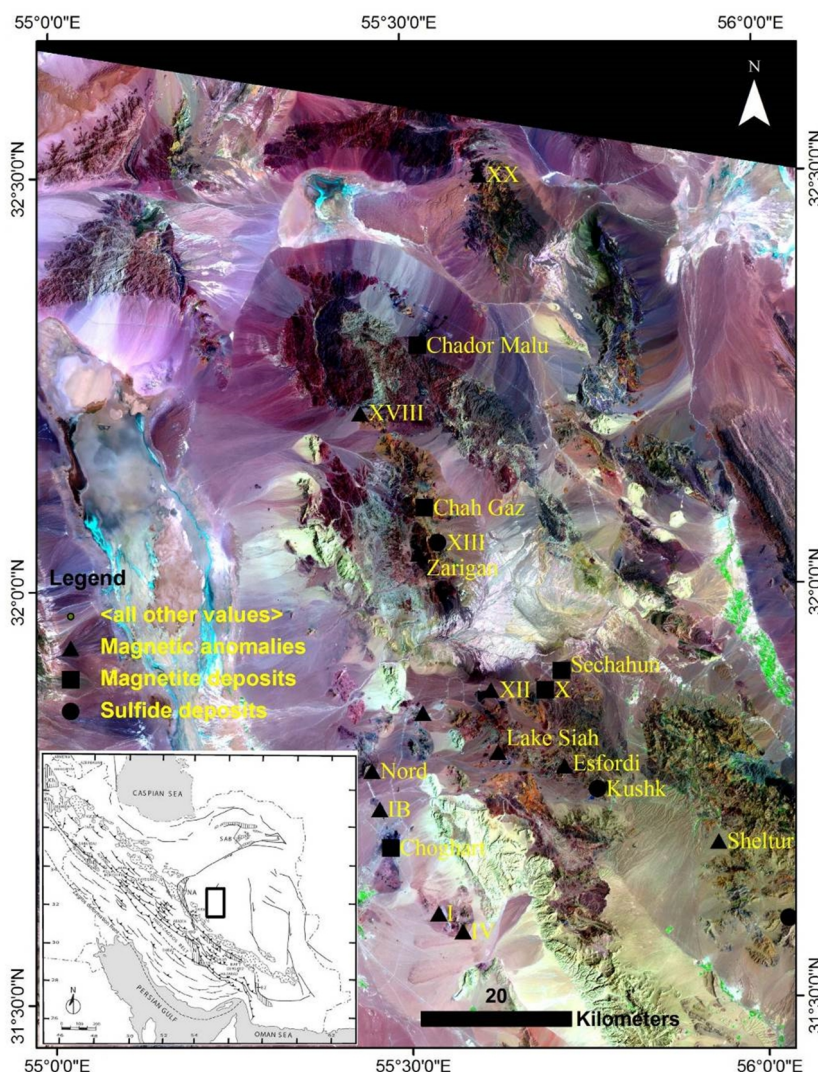


**Figure 3.** RGB color composite Landsat ETM<sup>+</sup> bands 7, 4, and 2 in which the different rock units in the study area are separated.

of the area is used to give a regional hint at the distribution of the rocks affected by alkali metasomatism. A summary of performance characteristics for ASTER and ETM+ sensors is given in Table. 2. The Aster sensor can achieve a high degree of accuracy in the spectral identification of rocks and minerals using absorption and reflection features in the SWIR region of the spectrum [21]. The SWIR bands are important for distinguishing Al-OH, Fe-OH, Mg-OH, H-O-H, and CO<sub>3</sub> absorption features associated with important alteration minerals such as illite/muscovite (sericite), kaolinite, epidote, calcite, and chlorite [21]. Such capability convinced the authors to use the Aster data in discriminating the special minerals characteristic of special altered areas and outcrops.

The remote sensing data for the study area were processed for alteration mapping with the particular aim of discriminating Th-bearing areas and associated alteration zones. To do this, several products including band ratios, false color composite image (using ETM+) and spectral angle mapper (using Aster images) were obtained.

**Color composites**

The human eye is capable of discriminating about 30 grey levels in the black-white range [14], it is much more sensitive to color differences and recognition of color patterns [4]. The false colors composite (FCC) image is one of the most rapid and useful methods for delineation of lithologic units [19]. Various researchers have proposed a range of FCC combinations prepared

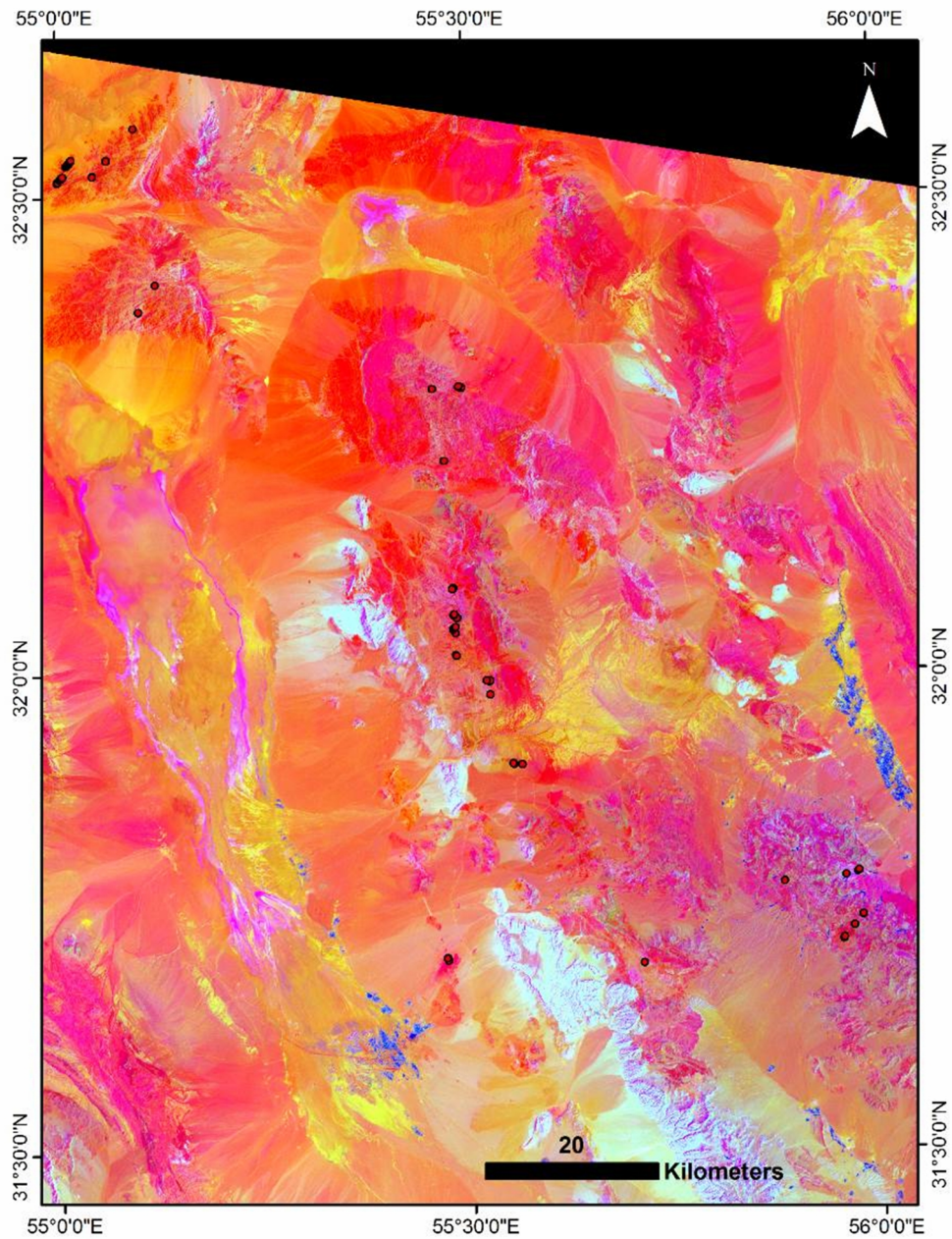


**Figure 4.** Landsat ETM<sup>+</sup> ratio image (bands 3/4, 5, and 5/7 in red, green, and blue, respectively) for the study area, showing the altered rocks as pale pink. The anomalies (red circles) are mainly located in the altered areas. Altered areas coincide with mountainous areas and show a remarkable decrease towards the northwest of the image.

using different bands. 7,4,2 Landsat ETM+ image, in this study, to separate the rock units, in common, and give us an overview of the distribution of the different rock units in the study area (Fig. 3). This color composite has widely been applied by several authors (e.g. Ranjbar et al, [39]; Yazdi et al, [51] among others) studied the areas containing a diversity of different rock types.

#### ***Band ratios***

Band ratios are radiometric and powerful tools for discriminating among mineral types in remote-sensing image data, by enhancing the spectral differences between bands and reducing the effects of topography ([40, 52]). Using this technique, bands with high reflectance are divided by bands with high absorption. The color composite of band ratio 3/4, band 5, and band ratio 5/7 is an example of ratio images that can be

displayed with the original bands [51]. This was the main band ratio used to reveal the altered rocks (Fig. 4). 5/7, 4/5 and 3/1 image was another band ratio product that gave an image very similar to the image obtained using 3/4, 5 and 5/7 band ratio, therefore was not cited in this study. Applying this method showed that the density of altered rocks decreases towards northwest that adopts with the observed northwestward declining of airborne Th anomalies.

Based on the field work and observations (next section) albitization and also actinolitization are observed in the study area particularly in the localities U-Th mineralization (which is thought to be, paragenetically, associated with REE mineralization) is occurred, but applying a field spectrometry program showed that U-Th mineralization is more coincide with the Na-metasomatism (characterized with albite) than actinolitization.

### ***Spectral Angle Mapper***

Since this research focuses on mapping the distribution of haloes of albitization that characterize, REE, U and Th mineralization, the prepared spectral in the spectral library characterize of selected alteration zones (albite) were used as reference spectra. In alteration zones found around the iron ore deposits, in the Bafq mining district, the alkali-metasomatism resulted in appearance of large amounts of albite and actinolite. REE, Th and U mineralization occurred along with this type of metasomatism. The SAM method was used to map the distribution of albite (and also actinolite) in their respective alteration zones (fig. 5). The Spectral Angle Mapper (SAM) is a tool that permits rapid mapping of the spectral similarity of image spectra to reference spectra [6]. This method assumes that the data have been reduced to apparent reflectance with all dark current and path radiance biases removed [29]. To manage the problem, some localities of Th mineralization coinciding with Na-metasomatism are selected in the present paper (Fig. 5). Looking at Fig. 5, it can be completely observed that the albitized areas host the rocks show traces of Th mineralization manifested on the airborne gamma spectrometry data. These data obtained through a gamma spectrometry program carried out by Prakla Seismos company (1976-1977) using NaI (TI) crystal (33.6 Litter) supervised by the atomic energy organization of Iran (AEOI). The observed geographical relationship between the albitized areas and the localities with high radioactivity points the presence of a genetic relationship between these two phenomena, albitization and Th mineralization. With

this framework, however, an interesting matter is that the albitization and Th mineralization correlates clearly with mountainous areas in a south-north (Fig. 5. A and B) to southwest-northeast (Fig. 5. B) arcuate trending pattern. This trending pattern correlates with the general arcuate trending pattern of the Paleozoic mountains in east central Iran formed during later phases of Pan-African orogeny. An interesting topic looking at this image (Fig. 5) is that the region show widespread areas underwent alkali-metasomatism characterized mostly by albite but, not all the albitized areas show high radioactivity. This matter has been investigated in several publications cited in this study and also examined in field observation carried out in this study. Albites are mainly of two types, the white ones that comprise most of the albites formed in this region and show no radioactivity or show weak radioactivity and the meaty ones that show high radioactivity and seem to be the main host of the radioactive bearing mineral phases. Therefore, logically, not all albitized areas show high radioactive intensity manifested on the airborne data. Similar images using the same technique (SAM) were also obtained in which the distribution of amphibole (actinolite) is shown (Fig. 6). Looking at Fig. 6 it can be observed that the areas show the distribution of albitization (in Fig. 5) also show the distribution of actinolitization that is logically attributed to presence of a paragenetic relationship between albite and actinolite in the Bafq region reported in previous studies and observed in this research.

### ***Field work and observation***

Based on the field observations and previous studies, alkali-metasomatism is the most spatially extensive and common type of metasomatism in the study area which is regionally observed and previously reported in several areas: Duzakh-Darreh area, Saghand ore field, Choghart, Chador-Malu, Esfordi, Se-Chahun and Chah Gaz mines. Amphibolytization (mostly actinolite) and albitization are the most prevalent results of alkali-metasomatism in this district. In this region alkali-metasomatism resulted in, paragenetically, formation of albite, amphibole (actinolite) in large amounts and argirine (alkali-pyroxene) in very limited amounts mainly observed in peripheral zones of iron ore deposits. According to Memar [30] the mineralization is of U-Th type in which davidite is the most common Ce-U bearing mineral found in part of the Saghand ore field affected by sodic metasomatism whereas in Choghart mine Th and REE-Th mineralization took place as thorite, thorigumite and monazite [28]. Remote sensing techniques, in addition to the field studies, were used to analysis the distribution of the

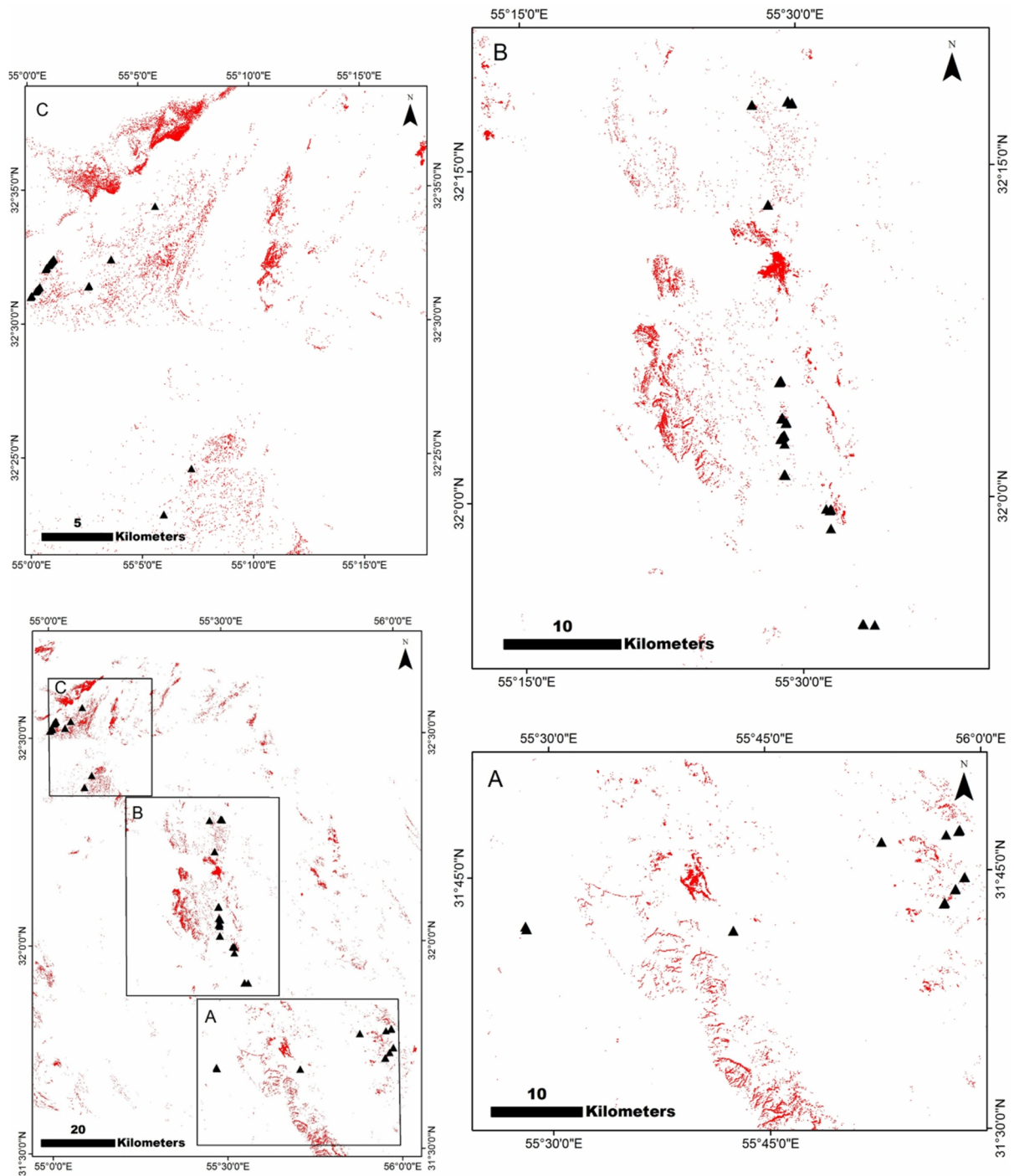


**Figure 5.** Plotting the radioactive airborne data (black triangles) on the distribution map of the areas containing high amounts of albite bearing rocks. This map compiled using spectral angel mapper (SAM) method. All the albitized areas do not show traces of radioactivity appeared on the airborne data (see the text for more discussion).

alkali metasomatism and its geochemical roles in distribution of the REE and Th prospects. The metasomatized rocks in the study area contain large amounts of actinolite and albite and also minor amounts

of tremolite, arfvedsonite, aegerine and biotite in widespread areas. To control the localities (on the images) affected by alkali matasomatism and, also, to evaluate the accuracy of the obtained results, two

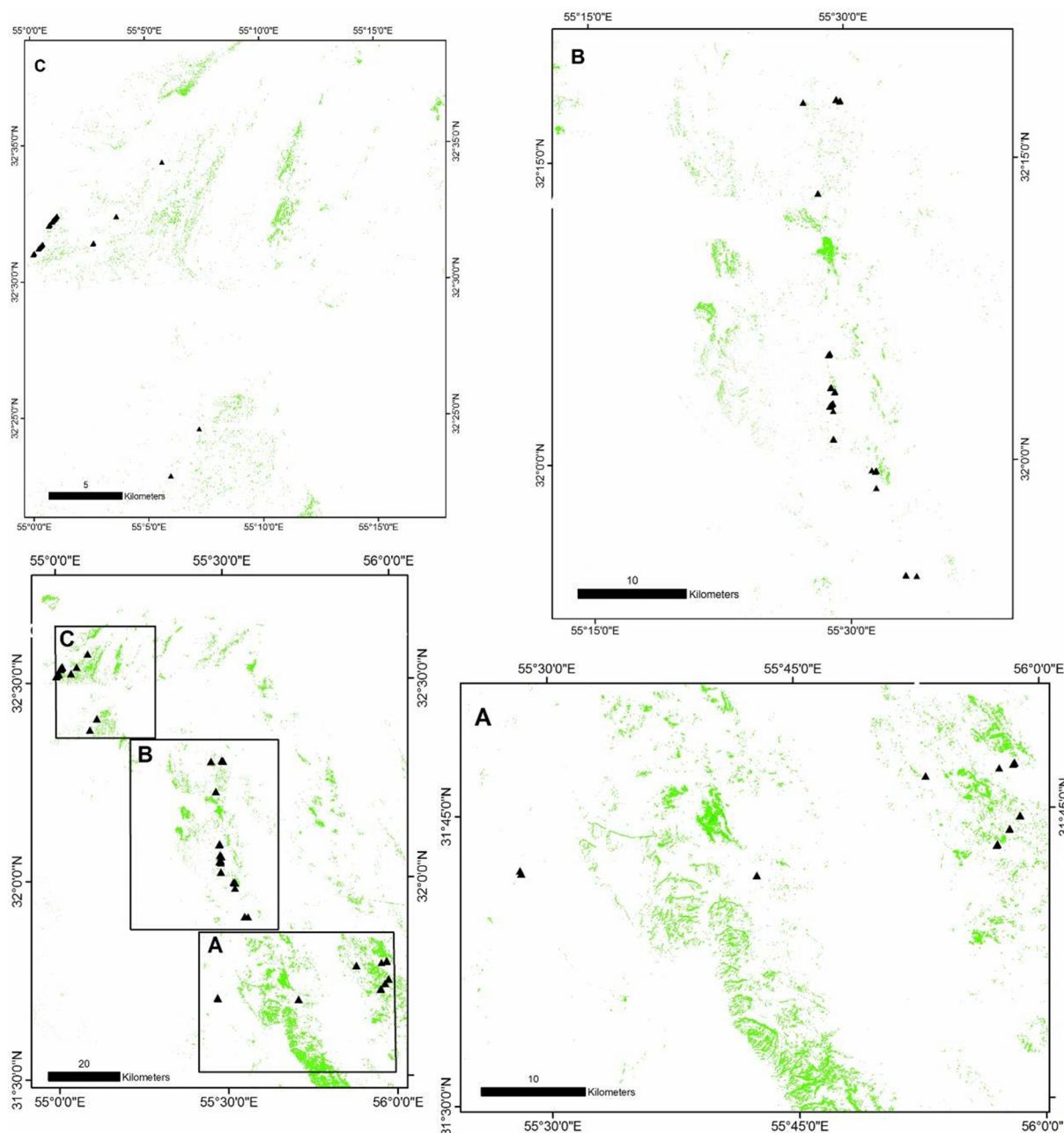


**Figure 6.** Plotting the radioactive airborne data (black triangles) on the distribution map of the areas containing high amounts of amphibol (actinolite) bearing rocks. This map compiled using spectral angel mapper (SAM) method. All the albitized areas do not show traces of radioactivity appeared on the airborne data (see the text for more discussion).

localities were studied, the Choghart iron mine (in the south-central part of the study area in Fig. 3) and the Saghand (in the north part of the study area in Fig. 3) Fe-U ore field. In the Bafq mining district alkali-metasomatism as amphibolytization and albitization has, paragenetically, occurred around the iron ore deposits. Such matter is more observed around iron deposits like anomaly 5 area in the vicinity of the

Saghand iron ore deposit (Fig 7. a and b). Albites are, genetically, of two types, the first in which the albites are white to pink in color found in surface and also deeper levels revealed on core samples drilled within and around metasomatic zones of iron ore deposits (Fig. 8. a) and the second that comprises the more reddish ones (meaty color) (Fig. 8. b). Field observations and ground spectrometry surveys, using RS-230

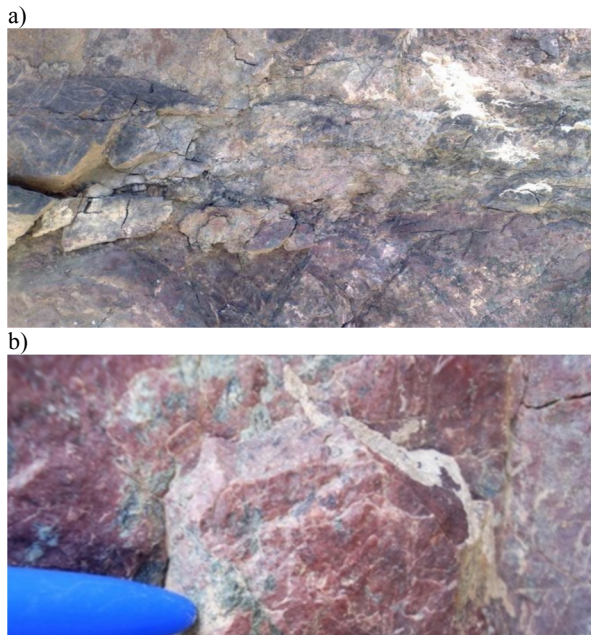


**Figure 7.** Distribution of alkali metasomatism in anomaly 5 area, Saghand ore field. a. Large masses of rocks affected by alkali metasomatic processes in which albitization is observed in a matrix, mineralogically, mostly composed of amphiboles (actinolite and tremolite). b. Close up view of the same phenomenon.

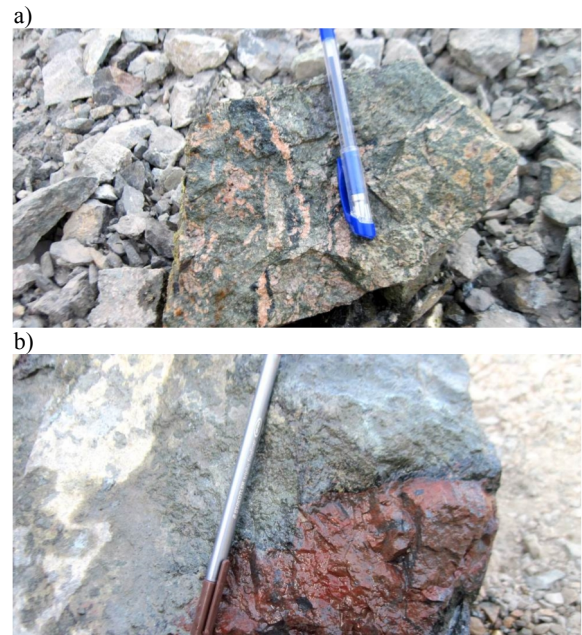


**Figure 8.** a. A typical core sample containing veinlets of white to pink albites in a matrix composed, dominantly, of actinolite. b. A patch of meaty albitite hosted in a rock composed, dominantly, of actinolite and minor meaty albitite.

spectrometer, revealed that the first type is characterized by radioactivity between 180-240cps (counts per second), whereas, the meaty ones show a radioactivity from 500 to more than 5000 cps. Results of chemical analysis using ICP-MS (inductively coupled plasma mass spectrometry) method on some taken samples collected from the metasomatized areas showed that the first albitite types with normal radioactivity lack any traces of REE and U-Th mineralization whereas the meaty ones show impregnations of REE- U-Th minerals. REE-U-Th mineralization is associated with this type of metasomatism in which amphybolitization and albitization affected large masses of rocks (Fig. 7).

## Results and Discussion

There has been an ongoing interest in the association of REE, natural radioactive elements and alkali-metasomatism in the last decades, noted in several publications (Kinnaird [27]; Cuney, et al [9]; Dahlkamp [10] among others). Geologically, most exposed REE and U-Th deposits have been explored in different geological environments using conventional methods and nowadays studies are focusing on the unexplored

resources through indirect techniques like airborne gamma spectrometry, radon surveys [23] and remote sensing, applied in this study. In this study, we used and combined several data layers including geologic map of the region (not cited herein), processed ETM+ and ASTER images and also airborne radiometric data, in Arc GIS (9.3) software to achieve a logical relationship among the available data to find a hint towards the factors controlling the REE and U-Th mineralization in the study area. Plotting these layers showed that the areas affected by hydrothermal alteration, in common, and alkali metasomatism, in particular, are well coincide with the areas show high radioactivity manifested in the airborne data. Large areas affected by actinolitization and albitization were revealed using remote sensing techniques but, field studies showed that not all of the albitized areas represent high radioactivity. High radioactivity was only observed in areas with extensive distribution of meaty albites.

Presence of the meaty albitite is a common aspect of albitization in the Bafq area noted in several areas. As was noted in previous sections, only the meaty albitites show high radioactivity which is, geochemically, related to processes affecting the rock bodies perhaps during a post-magmatic event in the study area, as is

suggested and discussed for similar areas studied in some parts of the world. According to Titayeva [47] and Pirajno [33] by the end of albitization processes, the thorium and uranium concentration increases. Part of REE and U-Th is retained in micro-fissures filled with hematite and chlorite. The reddish color is attributed to presence of micro-hematite in micro-fractures. Although, wilde [49] portrayed that the red or pink coloration is due to the presence of fine-grained disseminated hematite or hydrothermal apatite.

Reddish albites containing REE and U-Th mineralization are found mainly in Saghand ore field and Duzakh-Darreh areas whereas reddish albites containing Th-REE mineralization are found in the Choghart mine investigated critically in this study. Field observation and laboratory investigations revealed that albites from the Choghart mine contain REE and Th mineral inclusions that give albite a more reddish color [28].

### Acknowledgement

This paper is based on a part of the main author's Ph.D thesis at Shahid Beheshti university of Tehran, IR. Iran. This research was also supported by Nuclear Science & Technology Research Institute, AEOI and Shahid Beheshti university research center.

### References

1. Aghanabati A. Major sedimentary and structural units of Iran (map). *J. Geosci.* 7:29–30(1998).
2. Aghanabati A. Stratigraphy Encyclopedia of Iran: Precambrian to Silurian. Geological Survey of Iran and Mineral Exploration of Iran, Tehran, p. 658(2008).
3. Alavi M. Tectonic map of the Middle East (scale 1:5,000,000). Geological Survey and Mineral Exploration of Iran, Tehran(1991).
4. Ayalew Amara S. Spectral Remote Sensing of Hydrothermal Alteration Associated with Volcanogenic Massive Sulphide Deposits, Gorob-Hope Area, Namibia, MSc Thesis, Enschede, ITC, The Netherlands, 54p.(2007).
5. Bagheri S. and Stampfli G.M. The Anarak, Jandaq and Posht-e-Badam metamorphic complexes in Central Iran: new geological data, relationships and tectonic implications. *J. Tecton.* 451: 123–155(2008).
6. Becker H., Firsinger H. and Softel H. Central Iran, a former part of Gondwana? Palaeomagnetic evidence from Infra-cambrian rocks and iron ores of the Bafq area, central Iran, *J. ZGeo.* 39:953-963 (1973).
7. Boardman J. W. Spectral angle mapping: a rapid measure of spectral similarity (not published) (1993).
8. Borumandi H. Petrographische und lagerstättenkundliche Untersuchungen der Esfordi-Formation zwischen Mishdovaund Kushk bei Bafq (Zentraliran) Unpublished Ph.D. Thesis, Aachen, Germany, Rheinisch-Westfälische Technische Hochschule 174 p.(1973).
9. Cuney M., Emetz A., Mercadier J. and Mykchaylov V. Uranium deposits associated with Na-metasomatism from central Ukraine: A review of some of the major deposits and genetic constraints, *Journal of Ore Geology Reviews* 44:82-106 (2012).
10. Dahlkamp F. J. Uranium Ore Deposits, Springer-Verlag, Berlin, 460 p. (1993).
11. Daliran F. Kiruna-type iron oxide-apatite ores and 'apatites' of the Bafq district, Iran, with an emphasis on the REE geochemistry of their apatites. In: Porter, T. M. (Ed.), *Hydrothermal Iron Oxide Copper Gold and Related Deposits: A Global Perspective.*, 2. PGC Publishing, Adelaide, Australia, 303–320(2002).
12. Daliran F., Stosch H. G. and Williams P. A review of the Early Cambrian Magmatic and Metasomatic events and their bearing on the genesis of the Fe oxide-REE-apatite deposits (IOA) of the Bafq District, Iran. In: Williams, et al. (Eds.), *Smart Science for Exploration and Mining: Proceedings of the 10th Biennial SGA Meeting*, Townsville, Australia 17th–20th August (2009).
13. Daliran F., Stosch H. G., Williams P., Jamli, H. and Dorri M. B. Early Cambrian Iron Oxide–Apatite-REE (U) deposits of the Bafq district, East-Central Iran. In: Corriveau, L., Mumin, H. (Eds.), *Exploring for Iron Oxide Copper–Gold Deposits: Canada and Global Analogues. Geol Assoc Canada, Short Course Notes*, 20:143–155(2010).
14. Drury S. A. *Image Interpretation in Geology*. 3<sup>rd</sup> ed. Cheltenham: Nelson Thornes; Malden, MA. 304p. (2001).
15. Feldman G. K. About some varieties of spherulite quartz of the Zhovta Richka mine. Dnipropetrovsk: Bull Geol Mining circle of Dnipropetrovsk Mining Institute, 2(1926).
16. Forster H. Mesozoic-Cenozoic metallogenesis in Iran. *J. Geol. Soc.* 135:443-455(1978).
17. Forster H. and Jafarzadeh A. The bafq mining district in central iran a highly mineralized infracambrian volcanic field. *J. Econ. Geol.* 89:1697-1721(1994).
18. Gül M., Gürbüz K. and Kalelioglu Ö. Lithology Discrimination in Foreland Basin with Landsat TM. *J. Indian Soc. Remote Sens.* 40:257–269(2012).
19. Haghypour A. Geological map of the Biabanak-Bafq area, Geological Survey of Iran, scale 1:500000(1977).
20. Haghypour A. and Pelissier G. Geology of the Posht-e-Badam-Saghand area (east central Iran), *Iran Geological Survey Note* 48, 144 p.(1968).
21. Honarmand M., Ranjbar, H. and Shahabpour J. Combined use of ASTER and ALI data for hydrothermal alteration mapping in the northwestern part of the Kerman magmatic arc, Iran. *Int. J. Remote Sens.* 34:2023-2046(2013).
22. Huckriede R., Kursten M. and Venzlaff H. Zur geologie des gebiets zwischen Kerman und Saghand (Iran). *Beih. J. Geol. Jb.* 53:197(1962).
23. IAEA. *Advances in airborne and ground geophysical methods in uranium exploration IAEA nuclear energy series no. NF-T-1.5 Viena* (2013) 58p. (2013).
24. IAEA. *Uranium 2014; resources, production and demand.*

- 504p.( 2014).
25. Kargaranbafghi F., Neubauer F., Genser J., Faghieh A. and Kusky T. Mesozoic to Eocene ductile deformation of western Central Iran: From Cimmerian. *J. Tecton.* **564–565**: 83–100 (2012).
  26. Karimpour M. H., Malekzadeh Shafaroudi A., Stern C. R. and Hidarian M. R. Using ETM+ and Airborne Geophysics Data to Locating Porphyry Copper and Epithermal Gold Deposits in Eastern Iran. *J. Appl. Sci.* **8**:4004–4016(2008).
  27. Kinnaird J. A. Hydrothermal alteration and mineralization of the alkaline anorogenic ring complexes of Nigeria. *J. African Earth Sci.* **3**:229–252(1985).
  28. Khoshnoodi K. Mineralogy, geochemistry and genesis of radioactive elements in Choghart deposit, Bafq, central Iran, Ph.D Thesis, Shahid Beheshti University of Tehran, Iran, Not published(2014).
  29. Kruse F. A., Lefkoff A. B. Boardman J. B. Heidebreicht H. K. B. Shapiro A. T. Barloon P. J. and Goetz A. F. H. The spectral image processing system (SIPS)–interactive visualization and analysis of imaging spectrometer data. *J. Remote Sens. Environ.* **44**:145–63(1993).
  30. Memar A. Mineralogy and petrochemistry of a part of Saghand area, central Iran, Ph.D Thesis, University of Bombay, 150p. (1991).
  31. Mohammad Torab F. Geochemistry and metallogeny of magnetite-apatite deposits of the Bafq mining district, central Iran. Ph.d Thesis, Technical university of Claustal 131p. (2008).
  32. Nadimi A. Evolution of the Central Iranian basement. *J. Gondwana Res.* **12**: 324–333(2007).
  33. Pirajno F. Hydrothermal Processes and Mineral Systems. Springer 1250p. (2009).
  34. Rajabi A. Geology, mineralogy, texture and structure, geochemistry and genesis of Chahmir Zn-Pb deposit, south of Behabad, Yazd Province. M.Sc. thesis, Tarbiat Modares University, Iran (2008).
  35. Rajabi A. Ore controlling parameters and genesis of sedimentary-exhalative Zn-Pb (SEDEX type) deposits, Zarigan-Chahmir Area, East of Bafq, Central Iran. Ph.D. thesis, TarbiatModares University, Iran(2012).
  36. Rajabi A., Rastad E., Alfonso P. and Canet C. Geology, ore facies and sulfur isotopes of the Koushk vent-proximal sedimentary-exhalative deposit, Posht-e-Badam block, Central Iran. *Int. J. Geol. Rev.* **54**:1635–1648(2012).
  37. Rajabi A., Canet C., Rastad E. and Alfonso P. Basin evolution and stratigraphic correlation of sedimentary-exhalative Zn–Pb deposits of the Early Cambrian Zarigan-Chahmir basin, Central Iran. *J. Ore Geol. Rev.* **64**:328–353(2014).
  38. Ramezani J. and Tucker R. The Saghand region, central Iran: U-Pb geochronology, petrogenesis and implications for Gondwana Tectonics. *American J. Sci.* **303**(3):622–665(2003).
  39. Ranjbar H., Honarmand M. and Moezifar Z. Application of the Crosta technique for porphyry copper alteration mapping, using ETM data in the southern part of the Iranian volcanic sedimentary belt. *J. Asian Earth Sci.* **24**: 237-243 (2004).
  40. Rowan L. C. and Mars J. C. Lithologic mapping in the mountain pass, California, area using advanced space borne thermal emission and reflection radiometer (ASTER) data. *Remote Sens. Environ.* **84**:350–66(2003).
  41. Samani B., Saghand formation, a riftogenic unit of upper Precambrian in central Iran. *J. Geosci.* **6**: 32–45(1993).
  42. Sennewald S. and Kriiger T. Geologische und lager stitienkundliche Untersuchungen im Gebiet zwischen Kush und Se-Chahoon (Zentraliran)”: Unpublished Thesis, Aache Germany, Rheinisch-Westfalische Technische Hochschule, 210p.(1979).
  43. Stampfli G.M. Terranes Map of the Western Tethysides. UNIL, Université de Lausanne (open file) (2009).
  44. Stosch H. G., Romer R. I., Daliran F. and Rhede D. Uranium–lead ages of apatite from iron oxide ores of the Bafq District, East-Central Iran. *J. Mineralium Deposita.* **46**:9-21(2011).
  45. Taghipour S. "Genesis of apatite within Choghart, Chador-Malu and Esfordi iron oxides-apatite deposits, Bafq district, central Iran" Ph.D Thesis, university of Tehran, Iran, 150 p.(2013) (in persian).
  46. Tanatar I. I., “New rocks of the Kryvy Rig iron ore basin” Part1. *Injenerny Rabotnik* **7**(1925).
  47. Titayeva N. A. Nuclear geochemistry" CRC press 304p.(1994).
  48. Verdel C., Wernicke B.P., Renne, P.R. and Spell T.L. Geology and thermochronology of Tertiary Cordilleran-style metamorphic core complexes in the Saghand region of central Iran. *GSA Bull.* **119**: 961–977(2007).
  49. Wilde A. Towards a model for albitite-type uranium. *J. Miner.* **3**:36-48(2013).
  50. Yaghubpur A. and Mehrabi B. Koushk Zinc-Lead Deposit a typical black-shale-hosted deposit in Yazd State, Iran. *J. Sci., I.R.Iran* **8**(2):117–125(1997).
  51. Yazdi M., Taheri M., Navi p. and Sadati N. Landsat ETM<sup>+</sup> imaging for mineral potential mapping: application to Avaj area, Qazvin, Iran. *Int. J. Remote Sens.* **34**:5778–5795(2013).
  52. Zhang X., Pazner M. and Duke N. Lithologic and mineral information extraction for gold exploration using ASTER data in the south chocolate mountains (California). *ISPRS J. Photogram. Remote Sens.* **62**:271–82(2007).